J. Fluid Mech. (2026), *vol.* 1032, A63, doi:10.1017/jfm.2026.11419

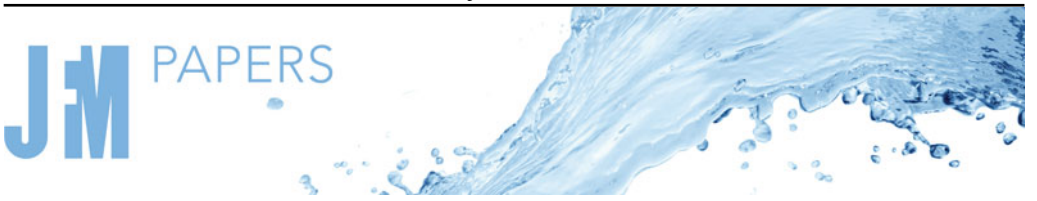

Self-lubricated spreading of nonpolar, surfactant-laden droplets

Yotam Stern[1], **Victor Multanen**[1], **Rafael Tadmor**[1] **and Roiy Sayag**[1,2,3]

[1]Department of Mechanical Engineering, Ben Gurion University of The Negev, Beer Sheva, Israel

[2]Department of Environmental Physics, Blaustein Institutes for Desert Research, Ben Gurion University of the Negev, Sede Boker, Israel

[3]Department of Physics, Ben Gurion University of the Negev, Beer Sheva, Israel

Corresponding authors: Roiy Sayag, roiy@bgu.ac.il; Rafael Tadmor, tadmorr@bgu.ac.il

(Received 10 December 2025; revised 30 January 2026; accepted 6 March 2026)

While surfactants are known to affect fluid–fluid interfaces, their impact on solid–liquid interfaces is an open problem. Here, we show that surfactants carried by a spreading nonpolar droplet can dynamically alter the solid–liquid interfacial energy, leading to a new spreading regime beyond the classical Tanner's law and known Marangoni regimes. We develop a theoretical framework that combines the new spreading mechanism, governed by the solid–liquid interfacial energy gradient, together with capillarity. Experiments across twelve distinct combinations of nonpolar solvents, surfactants, and substrates confirm our theoretical predictions for the transition from Tanner's law to the newly uncovered spreading regime. Our findings provide predictive control for applications in coatings, printing, microfluidics and surface engineering.

Key words: drops, interfacial flows (free surface), lubrication theory

1. Introduction

The dynamics of droplets that spread on solid surfaces is a long-studied topic which relates to various challenges in fluid dynamics (Hocking & Rivers 1982; Starov, Kalinin & Chen 1994; Tanner 1979; Bonn *et al.* 2009; Eggers *et al.* 2010; Sanjay & Lohse 2025; Stern *et al.* 2025*b*), including droplet bouncing (Stern *et al.* 2025*a*), emulsification processes (Stern *et al.* 2022) and droplet retraction (Tadmor *et al.* 2019, 2021). Central in this field is Tanner's law (Tanner 1979), which predicts that the base radius of a spreading droplet evolves in time t via a power law of $t^{1/10}$. This law is valid for spreading times exceeding an initial inertially dominated regime (Courbin *et al.* 2009), and is

© The Author(s), 2026. Published by Cambridge University Press. This is an Open Access article, distributed under the terms of the Creative Commons Attribution licence (https://creativecommons.org/licenses/by/4.0/), which permits unrestricted re-use, distribution and reproduction, provided the original article is properly cited.

https://doi.org/10.1017/jfm.2026.11419 Published online by Cambridge University Press

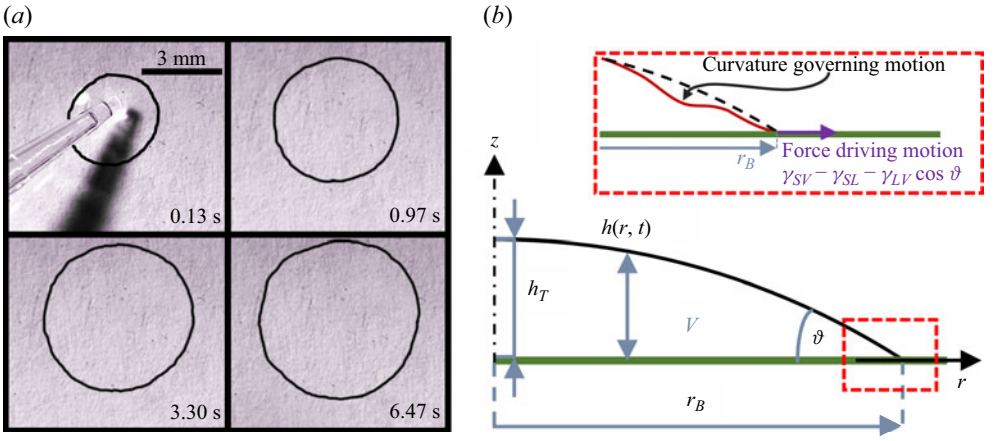

Figure 1. (*a*) Image sequence of a typical spreading experiment of a 2 µl, 6 mM octadecylamine-laden tetradecane droplet on mica (see movie 1). (*b*) Geometry of the axisymmetrically spreading droplet. The inset reveals the droplet shape near the propagating front r_B, where the force at the triple line leads to a curvature gradient (solid, red), in contrast to the approximate sketch (dash, black).

well established experimentally and theoretically for flows governed by visco-capillary forces. While Marangoni flow has been thoroughly explored (Marangoni 1871; Wei 2018; Rafaï *et al.* 2002), to date, no quantitative relation has been established between surfactant concentration and the spreading or retraction of droplets consisting of nonpolar solvents – which are free of Marangoni stresses unlike polar solvents – and notably, between surfactant adsorption and the gradients of the interfacial energies at solid–liquid interfaces. In contrast to Marangoni spreading, such as aqueous superspreading systems, where rapid spreading is driven by strong Marangoni stresses along the liquid–vapour interface (Wei 2018; Stoebe *et al.* 1996; Rafaï *et al.* 2002; Karapetsas, Craster & Matar 2011; Nikolov & Wasan 2011), the nonpolar solvents studied here exhibit no measurable surface tension gradients within our experimental resolution. The enhanced spreading reported below is instead associated with gradients in the solid–liquid interfacial energy, which act as a modification of the basal shear stress within the lubrication framework.

In this paper, we explore theoretically and experimentally the axisymmetric spreading of nonvolatile, surfactant-laden, nonpolar droplets. Our theory takes into account the forces that arise from the geometry of the droplet, capillarity and from the interaction of the surfactant carried by the droplet with the solid–liquid interface. Our experiments are performed on twelve distinct combinations of solvents, surfactants and substrates.

2. Non-Marangoni, visco-capillary spreading

We consider the axisymmetric spreading of a nonvolatile, nonpolar droplet of constant volume V and dynamic viscosity μ (figure 1). In a nonpolar solvent, the liquid–vapour surface tension remains constant, so that no Marangoni flow arises (Tadmor *et al.* 2021). The surfactants carried by the droplet can either remain in the bulk flow or be adsorbed onto the solid substrate. Owing to its spreading, the droplet base radius r_B, contact angle ϑ and thickness h (including top thickness, h_T, figure 1*b*) evolve in time t. We assume that the effect of gravity is negligible compared with surface tension (Starov *et al.* 1994), and are interested in finding the time evolution of $r_B(t)$.

In the case of fully wetting, surfactant-free droplets, spreading is driven by the motion of the contact line, via a force per unit length of $\gamma_{SV} - \gamma_{SL} - \gamma_{LV} \cos \vartheta$, where γ_{SV}, γ_{SL} and

https://doi.org/10.1017/jfm.2026.11419 Published online by Cambridge University Press

γ_{LV} are the solid–vapour, solid–liquid and liquid–vapour interfacial energies, respectively. This motion modifies the fluid thickness, leading to a gradient in the curvature of the liquid–vapour interface (figure 1*b*, inset) and resulting in a pressure gradient that governs the flow (Hocking & Rivers 1982; Starov *et al.* 1994). Modelling the flow via lubrication theory yields a nonlinear partial differential equation for $h(r, t)$

$$\frac{\partial h}{\partial t} + \frac{\gamma_{LV}}{3\mu r}\frac{\partial}{\partial r}\left(rh^3\frac{\partial}{\partial r}\left[\frac{1}{r}\frac{\partial}{\partial r}\left\{r\frac{\partial h}{\partial r}\right\}\right]\right) = 0, \tag{2.1a}$$

along with an integral equation representing global mass conservation

$$2\pi\int_0^{r_B} rh\,\mathrm{d}r = V. \tag{2.1b}$$

To close the problem, (2.1*a*) requires boundary conditions (BCs). As opposed to the case of gravity currents, where the BCs do not affect the bulk scaling (Hocking & Rivers 1982; Huppert 1982; Starov *et al.* 1994; Sayag & Worster 2013), one of these BCs is a contact-line condition that is required to regularise the moving-contact-line singularity (Voinov 1976; Cox 1986; King & Bowen 2001) and may thus introduce logarithmic corrections that involve a microscopic length scale. While these logarithmic corrections affect the scaling imposed by the bulk flow, they do not significantly change over the course of an experiment (§ S1 of the Supplementary Material (SM) available at https://doi.org/10.1017/jfm.2026.11419, Winkels *et al.* (2012)). Therefore, these corrections can be absorbed into the pre-factors of the scaling relations implied by the bulk equations (2.1)

$$h \sim \left(\frac{\gamma_{LV}}{\mu V^2}t\right)^{-1/5}; \qquad r_B \sim \left(\frac{\gamma_{LV}V^3}{\mu}t\right)^{1/10}, \tag{2.2}$$

where the pre-factors of order 1 depend on the BCs and can be found experimentally (Chen 1988) or estimated theoretically (Hocking & Rivers 1982; Starov *et al.* 1994). Equation (2.2) is often referred to as Tanner's law (Tanner 1979; Starov *et al.* 1994).

3. Faster spreading of surfactant-laden droplets

To explore the impact of surfactants on the propagation of nonpolar droplets in the absence of Marangoni stresses, we conduct laboratory experiments on nonvolatile, nonpolar solvents laden with surfactants. Specifically, we test octadecylamine-laden tetradecane droplets spreading on mica substrates (ODA/TD on mica) in a wide range of concentrations c_0 (between 0.6 and 148 mM) and volumes (between 1 µl and 4 µl). In each case, we mixed pure TD, which has $\gamma_{LV} \approx 26.56$ mJ m^{-2}, with ODA, and measured the evolution of the droplet radius from a top view (figure 1*a*). Combining our measurements together with available experimental data of the same system (Tadmor *et al.* 2019, 2020, 2021), we find that the spreading is consistent with Tanner's law at low surfactant concentrations ($c_0 \lesssim 12$ mM) (figure 2). In particular, the spreading in this regime reduces to a single master curve when normalised by $V^{3/10}$. However, at higher surfactant concentrations ($c_0 \gtrsim 12$ mM), we consistently obtain a power-law spreading of $t^{1/7}$. At the 'crossover' concentration of 12 mM the spreading evolution transitions during the experiment from $t^{1/10}$ at early times to $t^{1/7}$ at later times (figure 2*b*,*c*). In addition to the change in the scaling with respect to time for a certain concentration, we deduce a dependence of the spreading rate on the surfactant concentration for $c_0 \gtrsim 12$ mM, as evident by the parallel but not colinear trends in figure 2. To quantitatively assess these exponents, we performed global log–log regression fits over all data points in each regime.

https://doi.org/10.1017/jfm.2026.11419 Published online by Cambridge University Press

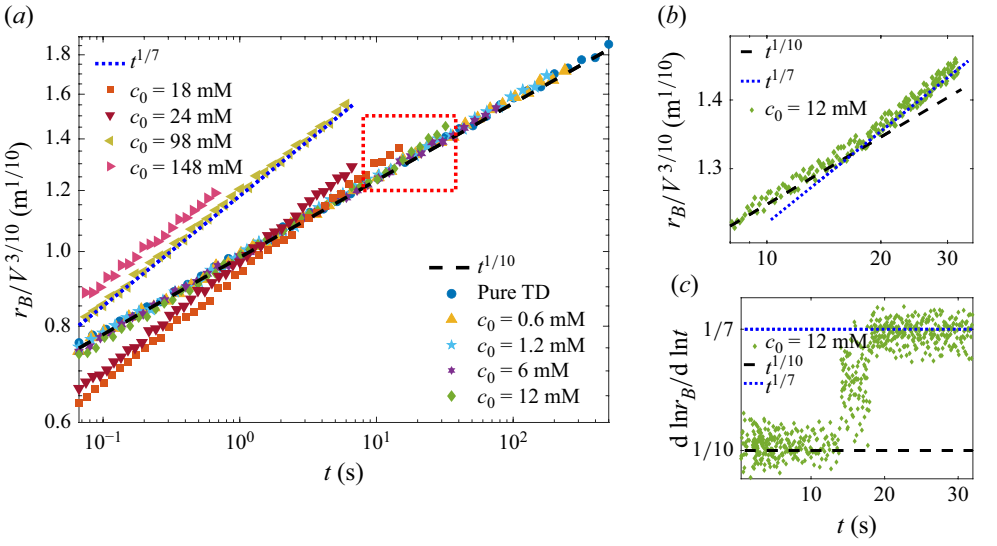

Figure 2. (*a*) Results of spreading experiments for ODA/TD on mica performed at a range of concentrations and volumes, showing $r_B/V^{3/10}$ against t on a log–log scale. Dashed lines follow trends corresponding to $t^{1/10}$ (black) and $t^{1/7}$ (blue), and the transition between them is revealed at the 'crossover' concentration (12 mM for this particular system): (*b*) a zoomed-in view of the crossover on a log–log scale; (*c*) the spreading exponent, obtained through $\mathrm{d}\ln r_B/\mathrm{d}\ln t$, plotted against time to validate the crossover between two distinct power-law trends.

The resulting best-fit exponents and 95 % confidence bounds (§ 2 of the SM) confirm consistency with $t^{1/10}$ in the Tanner regime and with $t^{1/7}$ in the surfactant-dominated regime.

Intriguingly, the 1/7 exponent that we measure does not correspond to the broad variety of Marangoni scaling laws in the literature (Rafaï *et al.* 2002; Wei 2018); particularly, while this 1/7 exponent is faster than Tanner's law, it is slower than the Marangoni exponents ranging between 1/6 and 1 (superspreading). We also note that across all concentrations, the surfactants did not alter γ_{LV}, which was measured before and after each experiment (Tadmor *et al.* 2021). Additionally, we distinguish our 1/7 exponent from the 1/7 exponent in two-dimensional droplets (Wei 2018) and molecular-kinetic theory models (de Gennes *et al.* 2004), which do not account for surfactant effects in contrast with our results that vary with c_0. Furthermore, the nonpolar solvent does not dissociate the substrate (Gee *et al.* 1990), and micelles cannot form; only inverted micelles, which do not impact surface tension or adsorption, can form (Tadmor *et al.* 2021). Therefore, our experimental results imply the existence of a surfactant-governed mechanism distinct from the known Marangoni laws, in which the main impact of the surfactants on the flow is through a non-uniform adsorption and subsequent modification of the solid–liquid interfacial energy (Tadmor *et al.* 2019, 2020, 2021).

4. Evidence of a γ_{SL} gradient and adsorption mechanism

4.1. *Experimental evidence of non-uniform adsorption and a γ_{SL} gradient*

To explore the hypothesised non-uniform surfactant adsorption and γ_{SL} posited in figure 3(*a*), we performed three independent experimental tests. First, we evaluated the presence of a surfactant monolayer on substrates using spectroscopic ellipsometry, finding a non-homogeneous surfactant monolayer whose density increased radially toward the

https://doi.org/10.1017/jfm.2026.11419 Published online by Cambridge University Press

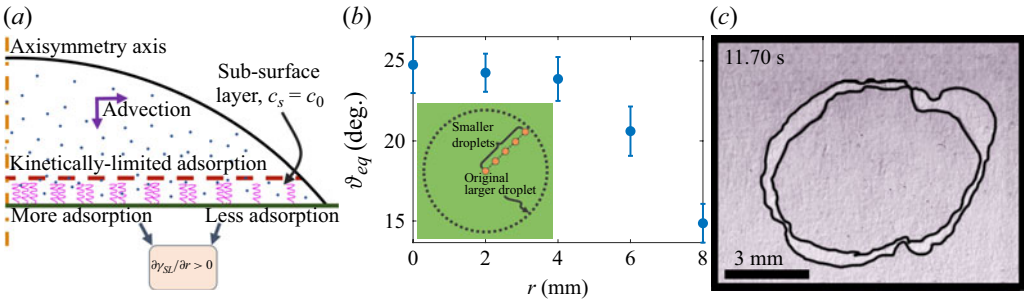

Figure 3. (*a*) Schematic description of the adsorption process and resulting γ_{SL} gradient. (*b*) Results of the big-droplet–small-droplet experiments (second γ_{SL}-gradient test), showing the radial decrease in the contact angle. Error bars indicate standard deviation over three trials. The inset shows schematically (not to scale) how smaller droplets were placed relative to the original larger droplet. (*c*) Separation of a droplet from a substrate by a uniform force (third γ_{SL}-gradient test), where the rim remaining attached demonstrates the interfacial energy gradient.

droplet centre across all samples (§ S3 of the SM, figure 3*a*). In the second test, we evaluated the non-uniformity of γ_{SL} by allowing a large (16 µl) surfactant-laden droplet (6 mM ODA/TD) to spread over a mica substrate for 10 s, removing it completely from the surface using a wipe (Kimwipe), then blowing compressed nitrogen on the substrate to remove excess microdroplets without altering it (de Gennes *et al.* 2004; Tadmor *et al.* 2019). Following this, we placed smaller droplets of pure TD at different radial locations relative to the original larger droplets (figure 3*b*, inset), and measured their equilibrium contact angles, ϑ_{eq}. This process was repeated three times for reproducibility. We observed that ϑ_{eq} grew larger closer to the centre of the original larger droplets (figure 3*b*). This implies a decreasing local γ_{SL} towards the centre of the larger droplets, so that $\partial\gamma_{SL}/\partial r > 0$ (§ S4 of the SM). In the third test, we separated surfactant-laden droplets from the substrate, while applying a uniform force, by attaching a Kimwipe, which was much larger than the droplet, to a rectangular slide, and observing that the separation was instantaneous. As the Kimwipe is much larger than the droplet and separation is rapid, the applied normal stress is effectively uniform; meanwhile, due to the instantaneous detachment, viscous relaxation during detachment is negligible, so that the measured force reflects the total adhesive resistance associated with variations in γ_{SL}. We observed that the core of the droplet detached, while a rim of fluid remained attached to the substrate (figure 3*c*). Since the applied force was uniform, this indicates weaker adhesion of the droplet centre to the substrate, implying lower γ_{SL} in that region, and stronger adhesion of the droplet front, implying a higher γ_{SL}.

Each of these three tests provides independent evidence of a positive radial gradient of γ_{SL}. Furthermore, the absence of any other notable difference with nonpolar, surfactant-free droplets leads to the ansatz that $\partial\gamma_{SL}/\partial r$ has dynamical consequences on spreading. We emphasise that a gradient seems crucial, as supported by evidence that a uniform γ_{SL} had no dynamical effect on the spreading of visco-gravity drops (Kumar *et al.* 2021).

4.2. *Surfactant transport and adsorption mechanism*

The formation of a radial gradient of γ_{SL} depends on the distribution of surfactants within the droplet and the adsorption mechanism. Initially, the surfactant is uniformly distributed in the droplet bulk at concentration c_0. The transport of surfactants in the bulk takes place via advection, to leading order (§ S5 of the SM). The timescales of radial and vertical advection scale like r/u and h/w, respectively, where u and w are the radial and

https://doi.org/10.1017/jfm.2026.11419 Published online by Cambridge University Press

vertical components of the fluid velocity, respectively, and by continuity the timescales are similar. Now, $r/u \propto r^4/h^3$, so that the time scale of advection, and in particular vertical advection, is larger near the front of the droplet than near the centre. Hence, the transport of surfactants to the solid–liquid interface is greater near the centre of the droplet and declines monotonically towards the droplet front.

The dominant adsorption mechanism in the experiments we consider is, to first order, Langmuir adsorption, consistent with the monolayers measured by ellipsometry (Tadmor *et al.* 2019, 2021; Xu *et al.* 2014). This adsorption mechanism is kinetically limited, where each surfactant molecule that adsorbs onto the substrate is immediately replaced in the sub-surface layer – the fluid layer adjacent to the substrate (figure 3*a*) – by another surfactant molecule (Diamant, Ariel & Andelman 2001; Tadmor *et al.* 2021), so that the sub-surface concentration c_s remains equal to c_0 throughout the spreading. This mechanism persists throughout spreading due to the efficient advection of surfactants, and the low loss of surfactants to the substrate relative to the initial amount of surfactants (Diamant *et al.* 2001; Tadmor *et al.* 2021). Consequently, the adsorption rate depends on c_0, the surface coverage (the local ratio between adsorption sites occupied by surfactants and total adsorption sites), and a rate constant $\bar{k}_{ads}$, which governs the relative affinity of the surfactant to adsorb to or desorb from the substrate (Diamant *et al.* 2001; Tabor, Eastoe & Dowding 2010; Tadmor *et al.* 2021). This results in a higher surface coverage near the centre of the droplet, where adsorption has been taking place since the inception of spreading and the vertical transport is higher, than near the front of the droplet, where adsorption initiates more recently and where vertical transport is weaker (figure 3*a*). Hence, we obtain that $\partial\gamma_{SL}/\partial r > 0$ throughout spreading, as γ_{SL} decreases with surface coverage.

5. Modelling the dynamical impact of γ_{SL} gradient on spreading

To model the effect of non-uniform γ_{SL} in our system, we consider the variation of the free energy of the solid–liquid interface, δE_{SL}, owing to a unit area displacement of the droplet $\mathrm{d}A$ and an interfacial energy increment $\Delta\gamma_{SL}$

$$\delta E_{SL} = \Delta\gamma_{SL}\mathrm{d}A. \tag{5.1}$$

As the change in the shear force $\mathrm{d}F$ is $-\partial E_{SL}/\partial r$, and the shear stress is $\mathrm{d}F/\mathrm{d}A$, a spatial gradient of γ_{SL} produces a tangential traction acting on the liquid through the interfacial layer of adsorbed surfactants adjacent to the solid. While the substrate itself is rigid and does not deform, adsorption-induced spatial variations in γ_{SL} modify the interfacial free energy and thereby result in a shear stress reduction on the liquid, analogous in form (but not in physical origin) to Marangoni stresses at liquid–vapour interfaces. Additionally, since the size of a surfactant molecule (at most a few nm) is negligible relative to the droplet thickness, we consider this shear stress reduction to be effectively on the solid substrate. Accordingly, the total tangential stress acting on the liquid at $z = 0$ is

$$\tau_{rz}|_{z=0} = \mu\left.\frac{\partial u}{\partial z}\right|_{z=0} - \frac{\partial\gamma_{SL}}{\partial r}. \tag{5.2}$$

Physically, a positive gradient of the solid–liquid interfacial energy reduces the friction experienced by the liquid at the substrate (figure 3), thereby promoting motion along the solid surface. Importantly, since the adsorption gradient extends over a finite region along the substrate behind the contact line, this effect modifies the basal stress over a

https://doi.org/10.1017/jfm.2026.11419 Published online by Cambridge University Press

macroscopic portion of the wetted area rather than acting solely as a localised contact-line forcing (as is the case in the aqueous superspreading systems mentioned in § 1). Therefore, we assume that a positive slip velocity, $u_s \triangleq u|_{z=0}$ exists, and is associated with an effective slip length β_{SL}, consistent with observed effects of a wettability gradient on the motion of droplets (de Gennes *et al.* 2004). We model the slip via a Navier-type condition (Hocking & Rivers 1982)

$$\mu \frac{\partial u}{\partial z}\bigg|_{z=0} \approx \mu \frac{u_s}{\beta_{SL}}. \tag{5.3}$$

Evaluating the Stokes equations under the lubrication approximation with a no-shear BC at the free surface, and combining (5.2) and (5.3) at the solid–liquid interface, yields

$$u_s = \frac{\beta_{SL}}{\mu}\left(h\frac{\partial}{\partial r}\left[\frac{\gamma_{LV}}{r}\frac{\partial}{\partial r}\left\{r\frac{\partial h}{\partial r}\right\}\right] + \frac{\partial \gamma_{SL}}{\partial r}\right), \tag{5.4}$$

which transforms the dynamic BC of (5.2) into the required kinematic BC for the Stokes equations (Shikhmurzaev 1997). Vertical integration of the local mass balance together with the radial flux leads to a new equation for $h(r, t)$

$$\frac{\partial h}{\partial t} + \frac{1}{\mu r}\frac{\partial}{\partial r}\left(rh\left[\left\{\frac{h}{3} + \beta_{SL}\right\} h\frac{\partial}{\partial r}\left\{\frac{\gamma_{LV}}{r}\frac{\partial}{\partial r}\left(r\frac{\partial h}{\partial r}\right)\right\} + \beta_{SL}\frac{\partial \gamma_{SL}}{\partial r}\right]\right) = 0, \tag{5.5}$$

which encodes a competition between capillarity and the γ_{SL} gradient, and also competition between h and β_{SL} within the capillary regime. To explore these competitions, we require a deeper understanding of β_{SL}, which we expect to be of the order of nanometres (hence $\ll h_T$) (Barrat & Bocquet 1999; Bocquet & Charlaix 2010). Even when $\partial\gamma_{SL}/\partial r$ dominates capillarity, spreading will decay if the droplet approaches Young's equilibrium, obtained at the equilibrium contact angle, ϑ_{eq}. In our experiments, $\vartheta_{eq} \ll \vartheta \ll 1$, so the force per unit length, $\gamma_{LV}(\cos\vartheta_{eq} - \cos\vartheta)$, representing the departure from Young's equilibrium, is approximated by $\gamma_{LV}\vartheta^2/2$. Therefore, $\beta_{SL} \propto \vartheta^2$, as has also been found experimentally in hydrophilic conditions (Barrat & Bocquet 1999; Bocquet & Charlaix 2010). Additionally, theory (Wörner *et al.* 2018) and experiments (Bocquet & Charlaix 2010) have shown that $\beta_{SL} \sim r_B$ for fixed ϑ. Consequently, $\beta_{SL} \sim r_B\vartheta^2$, implying that

$$\frac{\beta_{SL}}{r_B} \approx k_{SL}\left(\frac{h_T}{r_B}\right)^2, \tag{5.6a}$$

where k_{SL} is a dimensionless proportionality constant. The Langmuir adsorption mechanism implies the scaling $\Delta\gamma_{SL} \sim \bar{k}_{ads}c_0\gamma_{SL,0}$ (Diamant *et al.* 2001; Tabor *et al.* 2010), where $\gamma_{SL,0}$ is the initial solid–liquid interfacial energy. Therefore,

$$\beta_{SL}\frac{\partial \gamma_{SL}}{\partial r} \sim k_{SL}\left(\frac{h_T}{r_B}\right)^2 \bar{k}_{ads}c_0\gamma_{SL,0}. \tag{5.6b}$$

Considering the $h \ll \beta_{SL}$ limit, and scaling (5.5) in the capillarity-dominated case we reveal using (5.6*a*) that the spreading evolves like $r_B \propto t^{1/13}$, which we did not observe experimentally. This is consistent with our expectation that $h \gg \beta_{SL}$ holds for our experiments. In that limit, comparing the competing contributions of the solid–liquid interfacial energy and capillarity using (5.5) yields a new dimensionless number (§ S6 of

https://doi.org/10.1017/jfm.2026.11419 Published online by Cambridge University Press

the SM for further details)

$$I_J \triangleq \frac{r_B}{h_T}\frac{\gamma_{SL,0}}{\gamma_{LV}} k_{SL}\bar{k}_{ads}c_0, \tag{5.7}$$

which we term the Israelachvili number. This number is similar to the Marangoni number as it also compares an interfacial energy gradient with capillarity (Wei 2018). Here, I_J is the product of three factors: the first, $r_B/h_T \gg 1$, grows with time; the second, $\gamma_{SL,0}/\gamma_{LV}$, can span two to three orders of magnitude (ignoring liquid metals, which either do not wet substrates or form interfacial bonds with them, both beyond the scope of this work), and varies between ≈ 1.5 and ≈ 40 in our experiments (see § 6, § S2 of the SM). The third factor, $k_{SL}\bar{k}_{ads}c_0$, depends on k_{SL}, whose magnitude, while constant, is not yet known. The physical significance of this factor is the efficiency with which bulk surfactant concentration modifies the solid–liquid interfacial energy gradient thus reducing basal stress at the solid–liquid interface.

When $I_J \ll 1$, capillarity dominates, (5.5) simplifies to the visco-capillary model (2.1*a*), and r_B evolves via Tanner's law, as expected for low c_0; below a threshold concentration (e.g., $c_{0,T} \approx 6$ mM for ODA/TD on mica), I_J remains lower than 1 throughout spreading, and the spreading rate is independent of the initial surfactant concentration (figures 2, 4). Meanwhile, in the case of $I_J \gg 1$, where the $\partial\gamma_{SL}/\partial r$ dominates, our analysis yields a similarity scaling of the form

$$h \sim \left(\frac{k_{SL}\bar{k}_{ads}c_0\gamma_{SL,0}}{\mu V^{\frac{3}{2}}}t\right)^{-2/7} \quad ; \quad r_B \sim \left(\frac{k_{SL}\bar{k}_{ads}c_0\gamma_{SL,0}V^2}{\mu}t\right)^{1/7}, \tag{5.8}$$

which implies faster spreading at high surfactant concentrations relative to Tanner's law; above a higher threshold concentration (e.g. $c_{0,G} \approx 18$ mM for ODA/TD on mica), for which I_J is greater than 1 from very early times, the spreading evolves with the new 1/7 exponent throughout. We note that the spreading is proportional to $V^{3/10}$ and $V^{2/7}$ at low and high I_J, respectively, and as $3/10 \approx 2/7$, spreading is practically insensitive to the effect of volume relative to the effect of c_0.

Because I_J increases with time through the ratio r_B/h_T, we expect that for any nonpolar, surfactant-laden, nonvolatile droplet there is a range of crossover concentrations around a concentration c_{0,I_J} for which $I_J = 1$ at some time during spreading (provided Young's equilibrium is not reached beforehand). Spreading under such concentrations will initially follow Tanner's law ($I_J \ll 1$) and will later transition to a 1/7 exponent ($I_J \gg 1$). We observed such a path in our preliminary experiments, where $c_{0,I_J} = 12$ mM for ODA/TD on mica (figure 2*b*,*c*). Imposing $I_J = 1$ at $c_{0,I_J} \sim 10$ mM for ODA/TD on mica, and taking $r_B/h_T \gtrsim 10$, $\gamma_{SL,0}/\gamma_{LV} \approx 10$, $\bar{k}_{ads} \sim 10$ mM^{-1}, we obtain that $k_{SL} \sim 10^{-4}$. Consequently, (5.6*a*) and $r_B \gg h_T$ imply that β_{SL} is of the order of 1–10 nm, reaffirming that the $t^{1/13}$ scaling is not dominant in our system.

6. Universality of the new $t^{1/7}$ spreading law

To explore the universality of the impact of surfactants on the spreading of nonpolar droplets, we conducted experiments on a total of twelve different combinations of solvents (TD, dodecane (DD), hexadecane (HD)), substrates (mica, Au, Si) and surfactants (ODA, dodecylamine (DDA), sodium dodecyl sulphate (SDS), sodium dodecyl benzene sulphonate (SDBS)). The properties of all systems are provided in § S2 of the SM. For each experimental setting we performed experiments in a range of surfactant concentrations and

https://doi.org/10.1017/jfm.2026.11419 Published online by Cambridge University Press

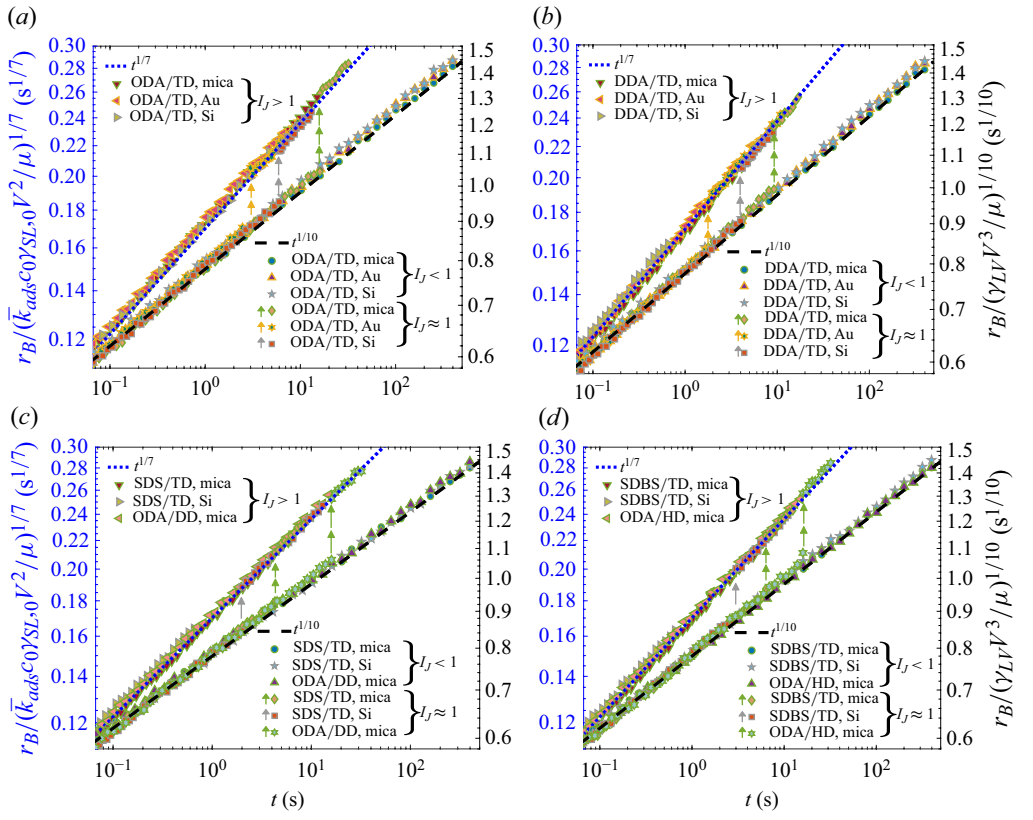

Figure 4. Similar measurements to those in figure 2 across 12 systems: (*a*) ODA/TD on mica, Au and Si (including all results presented in figure 2, e.g. the $c_0 \geqslant 18$ mM marker contains all concentrations 18–148 mM from figure 2), (*b*) DDA/TD on mica, Au and Si, (*c*) SDS/TD on mica and Si and ODA/DD on mica, (*d*) SDBS/TD on mica and Si and ODA/HD on mica. In each panel, the data are presented on two vertical axes; Right: data for $I_J \lesssim 1$, normalising r_B by $(\gamma_{LV}V^3/\mu)^{1/10}$. Left: data for $I_J \gtrsim 1$, normalising r_B by $(\bar{k}_{ads}c_0\gamma_{SL,0}V^2/\mu)^{1/7}$. Dashed lines correspond to trends of $t^{1/10}$ (black) and $t^{1/7}$ (blue). We mark transitions at $I_J \approx 1$ via arrows colour coded by substrate: mica (green), Si (grey), Au (gold).

volumes, measuring the evolution of the droplet radius as before. Additionally, γ_{LV} was measured before and after each experiment and no variations were recorded.

As shown in figure 4, we observe that all twelve experimental settings reduce to the same trends; below a range of 'transitional' concentrations, Tanner's law is followed, while above that range, the new 1/7 exponent arises. Equation (2.2) predicts that all data should collapse when r_B is normalised by $(\gamma_{LV}V^3/\mu)^{1/10}$ for $I_J \ll 1$; meanwhile, (5.8) predicts that all data should collapse when r_B is normalised by $(\bar{k}_{ads}c_0\gamma_{SL,0}V^2/\mu)^{1/7}$ for $I_J \gg 1$. These master-curve collapses are indeed shown in figure 4. Within the transitional range, arrows indicate the time when the spreading regime transitions from Tanner's law to the new 1/7 law. Moreover, we do not observe any other spreading evolution, and the value of $k_{SL} \approx 10^{-4}$ is confirmed across all the systems for which the rest of the parameters in I_J are known (Hołysz *et al.* 2008; Patil *et al.* 2010; You *et al.* 2016; Hartje *et al.* 2017; Holec *et al.* 2020; Fry *et al.* 2020). This suggests that k_{SL} is approximately constant for the wide class of substrates and liquids considered here. Once this parameter is fixed, the model quantitatively predicts the crossover via the criterion $I_J \sim 1$. This allowed us to determine the values of $\bar{k}_{ads}$ through c_{0,I_J} for systems in which it was unknown (§ S2 of the SM), and

https://doi.org/10.1017/jfm.2026.11419 Published online by Cambridge University Press

could be used to determine any unknown parameter in I_J, provided all other parameters are known.

Finally, although $h(r, t)$ was not measured explicitly, all droplets appeared parabolic throughout spreading, suggesting bulk self-similarity while also confirming that (5.8) is in agreement with our experiments through the global mass balance (2.1*b*). Since the substrate at the contact line is freshly wetted, adsorption behind the front does not directly modify the local interfacial energy and consequently the Young angle; thus, as in classical Tanner spreading, contact-line physics regularises the motion but does not determine the dominant bulk scaling.

7. Conclusions

We explore experimentally and theoretically the axisymmetric spreading of nonpolar, surfactant-laden droplets when volatility, gravity, Marangoni stresses and the initial inertio-capillary regime are neglected. We show, through twelve different experimental settings, that at higher surfactant concentrations a new non-Marangoni spreading of $r_B \propto t^{1/7}$ arises, while at lower concentrations Tanner's law of $r_B \propto t^{1/10}$ for surfactant-free droplets prevails. The new 1/7 exponent arises due to non-uniform surfactant adsorption to the substrate that forms a gradient in the solid–liquid interfacial energy. To explain these results, we formulate a new physical mechanism governing droplet spreading via a dynamic gradient in the solid–liquid interfacial energy. This yields a scaling of $r_B \propto (c_0 t)^{1/7}$, along with a newly discovered transition regime, spanning a range of surfactant concentrations, for which the power-law exponent transitions during the spreading from 1/10 (Tanner's law) to 1/7. The implication of the solid–liquid interfacial energy gradient is the reduction of interfacial shear stress and therefore of friction at the base of the droplet (at the sub-surface layer), which we model as partial slip at the solid–liquid interface. Our model therefore implies that a higher surfactant concentration leads to a stronger reduction in the basal stress. The significance of the solid–liquid interfacial energy gradient relative to capillarity is expressed through the Israelachvili number, I_J. This dimensionless number grows in time proportionally to the aspect ratio of the droplet, and also depends on the surfactant concentration and its affinity to be adsorbed onto the substrate. The Israelachvili number defines two different dynamical regimes: for $I_J \ll 1$, capillarity dominates and Tanner's law arises, while for $I_J \gg 1$, spreading is γ_{SL}-governed and follows the 1/7 power law. These two regimes are consistent with our experimental measurements, including the transition between regimes, which occurs due to the growth of I_J in time. This manifests the significance of the time-dependent quantity r_B/h_T to the spreading rate. We also note that contact-line regularisation may introduce logarithmic corrections to the spreading, but that these corrections do not significantly change over the course of the experiments, so that the leading-order spreading dynamics is accurately captured by the bulk flow. In future work, we intend to generalise these results by unifying this new spreading mechanism together with both capillarity and Marangoni flows.

Supplementary material and movie. Supplementary material and movie are available at https://doi.org/10.1017/jfm.2026.11419.

Acknowledgements. We acknowledge fruitful discussions with Dr. E. Boyko, Dr. Y. Green, and O. Lavi. We thank the Ilse Katz Institute for Nanoscale Science and Technology, whose nanofabrication centre provided us with Au surfaces. We also appreciate the skilful ellipsometry work performed by J. Jopp of the Ilse Katz Institute for Nanoscience and Technology. The Israelachvili number (IJ) is named in honour of Jacob N. Israelachvili, who first inspired R. Tadmor to study spreading and retracting droplets.

Funding. This research was supported in part by the Israel Science Foundation (Grant No. 730/22).

https://doi.org/10.1017/jfm.2026.11419 Published online by Cambridge University Press

Declaration of interests. The authors report no conflicts of interest.

References

BARRAT, J.-L. & BOCQUET, L. 1999 Large slip effect at a nonwetting fluid-solid interface. *Phys. Rev. Lett.* **82** (23), 4671–4674.

BOCQUET, L. & CHARLAIX, E. 2010 Nanofluidics, from bulk to interfaces. *Chem. Soc. Rev.* **39** (3), 1073–1095.

BONN, D., EGGERS, J., INDEKEU, J., MEUNIER, J. & ROLLEY, E. 2009 Wetting and spreading. *Rev. Mod. Phys.* **81** (2), 739–805.

CHEN, J.-D. 1988 Experiments on a spreading drop and its contact angle on a solid. *J. Colloid Interface Sci.* **122** (1), 60–72.

COURBIN, L., BIRD, J.C., REYSSAT, M. & STONE, H.A. 2009 Dynamics of wetting: from inertial spreading to viscous imbibition. *J. Phys.: Condens. Matter* **21** (46), 464127.

COX, R.G. 1986 The dynamics of the spreading of liquids on a solid surface. Part 1. Viscous flow. *J. Fluid Mech.* **168**, 169–194.

DIAMANT, H., ARIEL, G. & ANDELMAN, D. 2001 Kinetics of surfactant adsorption: the free energy approach. *Colloids Surf. A: Physicochem. Engng Aspects* **183–185**, 259–276.

EGGERS, J., FONTELOS, M.A., JOSSERAND, C. & ZALESKI, S. 2010 Drop dynamics after impact on a solid wall: theory and simulations. *Phys. Fluids* **22** (6), 062101.

FRY, B.M., MOODY, G., SPIKES, H.A. & WONG, J.S.S. 2020 Adsorption of organic friction modifier additives. *Langmuir* **36** (5), 1147–1155.

GEE, M.L., MCGUIGGAN, P.M., ISRAELACHVILI, J.N. & HOMOLA, A.M. 1990 Liquid to solidlike transitions of molecularly thin films under shear. *J. Chem. Phys.* **93** (3), 1895–1906.

DE GENNES, P.-G., BROCHARD-WYART, F. & QUÉRÉ, D. 2004 Transport phenomena. In *Capillarity and Wetting Phenomena: Drops, Bubbles, Pearls, Waves* (ed. P.-G. de Gennes, F. Brochard-Wyart & D. Quéré), pp. 261–287. Springer.

HARTJE, L.F., MUNSKY, B., NI, T.W., ACKERSON, C.J. & SNOW, C.D. 2017 Adsorption-coupled diffusion of gold nanoclusters within a large-pore protein crystal scaffold. *J. Phys. Chem. B* **121** (32), 7652–7659.

HOCKING, L.M. & RIVERS, A.D. 1982 The spreading of a drop by capillary action. *J. Fluid Mech.* **121**, 425–442.

HOLEC, D., DUMITRASCHKEWITZ, P., VOLLATH, D. & FISCHER, F.D. 2020 Surface energy of Au nanoparticles depending on their size and shape. *Nanomaterials* **10** (3), 484.

HOŁYSZ, L., MIROSŁAW, M., TERPILOWSKI, K. & SZCZEŚ, A. 2008 Influence of relative humidity on the wettability of silicon wafer surfaces. *Ann. UMSC Chem.* **63**, 223–239.

HUPPERT, H.E. 1982 The propagation of two-dimensional and axisymmetric viscous gravity currents over a rigid horizontal surface. *J. Fluid Mech.* **121**, 43–58.

KARAPETSAS, G., CRASTER, R.V. & MATAR, O.K. 2011 On surfactant-enhanced spreading and superspreading of liquid drops on solid surfaces. *J. Fluid Mech.* **670**, 5–37.

KING, J.R. & BOWEN, M. 2001 Moving boundary problems and non-uniqueness for the thin film equation. *Eur. J. Appl. Math.* **12** (3), 321–356.

KUMAR, P., ZURI, S., KOGAN, D., GOTTLIEB, M. & SAYAG, R. 2021 Lubricated gravity currents of power-law fluids. *J. Fluid Mech.* **916**, A33.

MARANGONI, C. 1871 Sul principio della viscosita' superficiale dei liquidi stabilito dalsig. *J. Plateau. Nuovo Cim* **5** (1), 239–273.

NIKOLOV, A. & WASAN, D. 2011 Superspreading mechanisms: an overview. *Eur. Phys. J. Spec. Top.* **197** (1), 325.

PATIL, K.G., SANTHANAM, V., BISWAS, S.K. & AYAPPA, K.G. 2010 Combined atomic force microscopy and modeling study of the evolution of octadecylamine films on a mica surface. *J. Phys. Chem. C* **114** (8), 3549–3559.

RAFAÏ, S., SARKER, D., BERGERON, V., MEUNIER, J. & BONN, D. 2002 Superspreading: aqueous surfactant drops spreading on hydrophobic surfaces. *Langmuir* **18** (26), 10486–10488.

SANJAY, V. & LOHSE, D. 2025 Unifying theory of scaling in drop impact: forces and maximum spreading diameter. *Phys. Rev. Lett.* **134** (10), 104003.

SAYAG, R. & WORSTER, M.G. 2013 Axisymmetric gravity currents of power-law fluids over a rigid horizontal surface. *J. Fluid Mech.* **716**, R5.

SHIKHMURZAEV, Y.D. 1997 Spreading of drops on solid surfaces in a quasi-static regime. *Phys. Fluids* **9** (2), 266–275.

STAROV, V.M., KALININ, V.V. & CHEN, J.-D. 1994 Spreading of liquid drops over dry surfaces. *Adv. Colloid Interface* **50**, 187–221.

https://doi.org/10.1017/jfm.2026.11419 Published online by Cambridge University Press

STERN, Y., FROG, I., MULTANEN, V., HANANOVITZ, M., VINOD, A. & TADMOR, R. 2025*a* Probabilistic droplet bouncing. *Phys. Fluids* **37** (12), 121702.

STERN, Y., TADMOR, R., MIRON, A. & VINOD, A. 2025*b* Furmidge equation revisited. *Langmuir* **41** (18), 11785–11793.

STERN, Y., TADMOR, R., MULTANEN, V. & OREN, G. 2022 A first order-based model for the kinetics of formation of Pickering emulsions. *J. Colloid Interface Sci.* **628**, 409–416.

STOEBE, T., LIN, Z., HILL, R.M., WARD, M.D. & DAVIS, H.T. 1996 Surfactant-enhanced spreading. *Langmuir* **12** (2), 337–344.

TABOR, R.F., EASTOE, J. & DOWDING, P.J. 2010 A two-step model for surfactant adsorption at solid surfaces. *J. Colloid Interface Sci.* **346** (2), 424–428.

TADMOR, R., BAKSI, A., GULEC, S., JADHAV, S., N'GUESSAN, H.E., SOMASI, V., TADMOR, M., TANG, S., WASNIK, P. & YADAV, S. 2020 Defying gravity: drops that climb up a vertical wall of their own accord. *J. Colloid Interface Sci.* **562**, 608–613.

TADMOR, R., BAKSI, A., GULEC, S., JADHAV, S., N'GUESSAN, H.E., SEN, K., SOMASI, V., TADMOR, M., WASNIK, P. & YADAV, S. 2019 Drops that change their mind: spontaneous reversal from spreading to retraction. *Langmuir* **35** (48), 15734–15738.

TADMOR, R., MULTANEN, V., STERN, Y. & YAKIR, Y.B. 2021 Drops retracting while forming a rim. *J. Colloid Interface Sci.* **581**, 496–503.

TANNER, L.H. 1979 The spreading of silicone oil drops on horizontal surfaces. *J. Phys. D: Appl. Phys.* **12** (9), 1473.

VOINOV, O.V. 1976 Hydrodynamics of wetting. *Fluid Dyn.* **11** (5), 714–721.

WEI, H.-H. 2018 Marangoni-enhanced capillary wetting in surfactant-driven superspreading. *J. Fluid Mech.* **855**, 181–209.

WINKELS, K.G., WEIJS, J.H., EDDI, A. & SNOEIJER, J.H. 2012 Initial spreading of low-viscosity drops on partially wetting surfaces. *Phys. Rev. E* **85** (5).

WÖRNER, M., CAI, X., ALLA, H. & YUE, P. 2018 A semi-analytical method to estimate the effective slip length of spreading spherical-cap shaped droplets using Cox theory. *Fluid Dyn. Res.* **50** (3), 035501.

XU, Y., LIU, Y.-L., GAO, S., JIANG, Z.-W., SU, D. & LIU, G.-S. 2014 Monolayer adsorption of dodecylamine surfactants at the mica/water interface. *Chem. Engng Sci.* **114**, 58–69.

YOU, H., LIU, X., LIU, H. & FANG, J. 2016 Theoretical description of the role of amine surfactant on the anisotropic growth of gold nanocrystals. *CrystEngComm* **18** (21), 3934–3941.

https://doi.org/10.1017/jfm.2026.11419 Published online by Cambridge University Press